Thiophenesulfonamides are specific inhibitors of quorum sensing in pathogenic Vibrios

Jane D. Newman[1], Priyanka Shah[2], Jay Chopra[2], Eda Shi[2], Molly E. McFadden[3], Rachel E. Horness[4], Laura C. Brown[4*], Julia C. van Kessel[1*]

1. Department of Biology, Indiana University, Bloomington, IN 47405, USA
2. Current institution: Indiana University School of Medicine, Indianapolis, IN 46202, USA
3. Current institution: California Institute of Technology, Pasadena, CA 91125, USA
4. Department of Chemistry, Indiana University, Bloomington, IN 47405, USA

* Corresponding authors:

Julia van Kessel

Email: jcvk@indiana.edu

Telephone: 812-856-2235

Laura Brown

Email: brownlcb@indiana.edu

Telephone: 812-856-5620

Abstract

Vibrio bacteria are pathogens of fish, shellfish, coral, and humans due to contaminated seafood consumption. *Vibrio* virulence factors are controlled by the cell-to-cell communication called quorum sensing, thus this signaling system is a promising target for therapeutic design. We screened a compound library and identified nine compounds, including several 2-thiophenesulfonamides, that inhibit the master quorum sensing transcription factor LuxR in *Vibrio campbellii* but do not affect cell growth. We synthesized a panel of 50 thiophenesulfonamide compounds to examine the structure-activity relationship effects on quorum sensing *in vivo*. The most potent molecule identified, PTSP (3-phenyl-1-(thiophen-2-ylsulfonyl)-1*H*-pyrazole), specifically inhibits LuxR homologs in multiple strains of *Vibrio vulnificus*, *Vibrio parahaemolyticus*, and *V. campbellii* with sub-micromolar concentrations. PTSP efficacy is driven by amino acid conservation in the binding pocket, which is accurately predicted using *in silico* modeling of inhibitors. Our results underscore the potential for developing thiophenesulfonamides as specific quorum sensing-directed treatments for *Vibrio* infections.

Introduction

Vibrio species are principal pathogens of marine animals, including fish, shellfish, and coral. Global warming and the concomitant rise of ocean temperatures correlates with increases in *Vibrio* prevalence and spread to regions beyond their typical equatorial habitats[1-3], consequently harming fish and shellfish aquaculture industries and natural marine ecosystems worldwide. Thus, there is a global need for new treatments for vibriosis in coral reef ecosystems, aquaculture, and in human health, due to consumption of contaminated fish and shellfish. In pathogenic marine *Vibrio* species studied to date, the bacterial cell-cell signaling system called quorum sensing controls biofilm formation, as well as expression and secretion of virulence factors[4,5]. Quorum sensing involves the production and detection of signaling molecules called autoinducers that provide information about the number and type of bacterial cells in the near vicinity. As populations of cells grow more dense, autoinducer concentrations increase, and detection of these molecules drives changes in gene expression to alter population-wide behaviors, including those required for pathogenesis.

In vibrios, autoinducers are sensed by membrane-bound histidine kinase receptors that participate in a phosphorylation cascade, ultimately controlling production of the master regulator LuxR (Fig. 1)[5-7]. At low cell densities (LCD), low levels of LuxR are produced. At high cell densities (HCD), maximal LuxR protein is produced, and this transcription factor activates and represses hundreds of genes[8]. Although the number and type of autoinducers and receptors vary among vibrios, the LuxR protein is highly conserved in all pathogenic vibrios studied to date[9-14]. Although the naming of the *V. campbellii* protein LuxR causes confusion, this protein does not resemble or function like the LuxR protein that is part of the *Vibrio fischeri* LuxI/LuxR quorum sensing system, which requires binding to the autoinducer molecule made by LuxI for activity[15]. Conversely, the LuxR from *V. campbellii* belongs to the TetR superfamily[16], and these proteins are structurally, genetically, biochemically, and functionally distinct from the

V. fischeri LuxR. LuxR/TetR homologs in vibrios include SmcR in *V. vulnificus*, HapR in *V. cholerae*, OpaR in *V. parahaemolyticus*, and VcpR in *Vibrio coralliilyticus*, which share 76-96% amino acid identity[14]. The LuxR/TetR-type proteins do not have a known ligand, although a putative ligand binding pocket has been defined in structures and shown to bind inhibitors[17-19]. LuxR/TetR proteins in vibrios directly bind to multiple sites in promoter regions and interact with other proteins (*e.g.*, RNA polymerase, IHF) or compete with other proteins (*e.g.*, H-NS) to activate or repress transcription of hundreds of quorum sensing genes[6,8,20-22].

Vibrio LuxR/TetR-type proteins play crucial roles in colonization and infection of hosts through quorum-directed regulation of biofilm formation, type III and type VI secretion systems, motility, and production of proteases, hemolysins, siderophores, and cytotoxins[4]. Deletion or inhibition of LuxR proteins in several vibrios reduces or eliminates colonization and toxicity, effectively increasing host survival[11,17,23]. Thus, LuxR represents a key target for designing therapeutics to block quorum sensing in vibrios. LuxR inhibitors would presumably render *Vibrio* cells unresponsive to quorum sensing signals even at HCD, thus restricting cells to their LCD gene expression program. Indeed, recent studies have shown that quorum sensing inhibitors are viable alternative approaches to traditional antibiotics in disease treatment with demonstrated efficacy in animal models and active clinical trials[24,25]. Because quorum sensing inhibitors typically do not affect growth of the bacteria but rather inhibit specific pathways[26,27], these molecules are hypothesized to generate less selective pressure for evolving resistance.

V. campbellii LuxR-specific inhibitors have been identified via a variety of methods, including both *in vitro* and *in silico* screening strategies. These include compounds with varying functional groups such as aromatic enones, sulfonamides, sulfones, cinnamaldehydes, furanones, and brominated thiophenones[28-33], and each was shown to specifically inhibit bioluminescence, biofilm formation, and/or protease activity in *V. campbellii* and in some cases other *Vibrio* species. However, the range of inhibition for some of these molecules is either low (~3-fold) or the inhibitory concentrations required to observe phenotypic effects *in vitro* or *in vivo* are high

(>20 μM). Several of these molecules show favorable therapeutic potential because addition of these molecules to brine shrimp larvae infected with *Vibrio* cells increases survival. In particular, the molecule called Qstatin (1-((5-bromothiophen-2-yl)sulfonyl)-1*H*-pyrazole) is a highly promising molecule that was shown to be a specific inhibitor of the LuxR homolog SmcR in *Vibrio vulnificus* both *in vitro* and *in vivo*[17].

Here, we used an *E. coli* bioassay to screen chemical libraries to identify specific inhibitors of LuxR that do not affect bacterial cell growth. Our structure-activity relationship data shows that multiple thoiphenesulfonamide-containing molecules with heterocycle variations are strong inhibitors of LuxR-type proteins in a wide-range of pathogenic *Vibrio* species.

Results

A bioassay screen identifies LuxR chemical inhibitors

LuxR proteins activate and repress gene expression in vibrios through direct binding to specific DNA sequences in promoters[6,14,22]. Previously, we developed a bioassay that consists of a dual-color fluorescent reporter plasmid that reports both LuxR activities: the *luxCDABE* promoter is activated by LuxR and drives expression of *gfp*, and the *VIBHAR_05222* promoter is repressed by LuxR and drives expression of *mCherry*[22] (Fig. 2A). We use this reporter plasmid in an *E. coli* strain that also contains a plasmid expressing LuxR from its native promoter. Thus, in the presence of LuxR, GFP levels increase and mCherry levels decrease compared to the control strain (Fig. 2B). As a positive control, we showed that Qstatin inhibits LuxR activity in this assay (Fig. S1). We screened ~60,000 molecules in the ChemBridge (Fig. S1A, S1C) and Chemdiv (Fig. S1B) libraries and identified nine compounds that inhibit LuxR activation and/or repression but do not affect the final growth yield more than 10%. Four of these compounds contain a sulfonamide or sulfamide core with variable groups on each side similar to Qstatin, whereas the other compounds are structurally dissimilar (Fig. 2C). We synthesized or purchased these molecules and determined the IC_{50} for each in the *E. coli* bioassay strain using

titration curves (Table S1, Fig. 2D, 2E). P0053 I18 has the best inhibitory effect on LuxR in the *E. coli* bioassay with an IC_{50} similar to Qstatin (Table S1, Fig. 2D, 2E). P2065 E16 has only a minor inhibition of LuxR, and a variation of this molecule lacking the CF_3 group on the heterocycle has no activity (Fig. 2D, 2E). We also observed consistent though low inhibition by P0074 H04 and P0053 O05, which also contain sulfamide/sulfonamide cores (Fig. 2D, 2E).

2-thiophenesulfonamide compounds specifically inhibit LuxR

To further explore the thiophenesulfonamide class of compounds that includes Qstatin and P0074 H4, we synthesized a panel of Qstatin derivatives with steric and electronic structural variations in both heterocycles (Fig. 3A). We refer to modifications to the heteroaromatic amine ring (pyrazole in the case of Qstatin) with number designations for each class and modifications to the thiophene ring with letter designations for each class (Fig. 3A). Assays with these molecules in the *E. coli* bioassay showed that the most active compounds contain a 3-methyl- (class 8) or 3-phenyl-substituted pyrazole (class 10), an unsubstituted pyrazole (class 1), or a pyrrole in place of the pyrazole (class 3) (Fig. 3B, 3C, S2). Compounds containing other heterocycles do not have activity against LuxR (Fig. S2). It is particularly noteworthy that the compounds containing an imidazole ring (class 2) are not active given that the structure is highly similar to pyrroles and pyrazoles (classes 1 and 3). Methyl substitution at the 3 position of the pyrazole does not alter activity compared to Qstatin (class 8), however methyl substitution at both the 3- and 5- positions of the pyrazole eliminates activity (class 9). In most cases, the presence/absence of Br or Cl atoms on the thiophene ring does not alter activity (Fig. 3). For example, Qstatin, 1B, and 1C have similar activities, and 10A, 10B, and 10C have similar activities. The conformation of the sulfonamide core appears to be critical because substitution with a carbonyl eliminated activity of that class of compounds (classes F and G). The most potent molecules are compounds 10A, 10B, and 10C, all of which contain a

148 phenyl group on the 3- position of the pyrazole and vary in the presence or absence of bromine
149 or chlorine on the thiophene ring (Fig. 3, S2).

150 Many sulfonamide-containing compounds are known to target the folate synthesis
151 pathway in bacteria and inhibit growth (bacteriostatic), and thus these “sulfa drugs” have been
152 used as broad-spectrum antibiotics for decades[34,35]. However, the structurally distinct 2-
153 thiophenesulfonamides generally do not have any bacteriostatic activity; only two compounds
154 (4A and 4C) in this entire panel limit *E. coli* growth yield more than 10% compared to negative
155 controls, and this effect was only observed at concentrations of 100 μM and higher (Fig. S3A).
156 Addition of high concentrations of 10B or 10C to *V. campbellii* or *V. vulnificus* does not alter
157 growth rate or growth yield (Fig. S3B, 3C), suggesting that the inhibitory activity is specific to
158 LuxR, and these are not general antibacterial compounds. Indeed, RNA-seq performed with
159 Qstatin showed a specific effect on the SmcR regulon[17]. Further, we note that molecule 10B
160 inhibits LuxR activity rapidly; GFP production is blocked 120 minutes after 10B addition to the
161 culture, and this is maintained until 16 hours (Fig. S3D). Collectively, these data show that 2-
162 thiophenesulfonamide molecules are stable in bacterial culture, specifically inhibit LuxR, and do
163 not significantly affect cell growth.
164
165 *2-thiophenesulfonamides inhibit quorum sensing in Vibrios*
166 Qstatin has been shown to be an effective inhibitor of SmcR *in vitro* and *in vivo*[17]. It also
167 inhibits pathogenesis in *V. campbellii*, *V. parahaemolyticus*, and *V. vulnificus* in a shrimp
168 infection assay, presumably through inhibition of the LuxR-type protein in these strains[17]. To
169 assess the activity of our panel of thiophenesulfonamide inhibitors against other vibrios, we
170 assayed quorum-sensing controlled phenotypes in several strains from five *Vibrio* species: *V.*
171 *campbellii, V. coralliilyticus, V. cholerae, V. parahaemolyticus,* and *V. vulnificus*. Although most
172 of these vibrios are not bioluminescent, the *luxCDABE* operon from *V. campbellii* BB120 is
173 routinely used to measure quorum sensing and LuxR regulation in other vibrios because LuxR

174 directly binds this promoter and is required for gene expression[17,36-39]. We introduced a plasmid
175 containing the *luxCDABE* promoter driving expression of *gfp* (pCS19 (kanamycin-resistance
176 cassette) or pCS42 (gentamicin-resistance cassette)) into each of the *Vibrio* strains. We
177 focused our assays on the molecules with the most activity determined in Fig. 3, which we refer
178 to as the "top panel". We observed that 10A, 10B, and 10C molecules are the most inhibitory in
179 *V. campbellii*, *V. vulnificus*, and *V. parahaemolyticus*, and in each, 8A has a similar IC_{50} to
180 Qstatin (Fig. 4A-E, Table S2). Molecules 10A, 10B, and 10C are so potent in *V. vulnificus* that
181 we performed extended serial dilutions to obtain accurate IC_{50} data because initial titrations did
182 not yield enough points for a complete curve (Fig. 4E, S4A-C, Table S2). We also observed that
183 few molecules are active in *V. coralliilyticus* OCN008, but 3B has the most noticeable effect
184 (Fig. 4C). Importantly, there is a distinct difference in the half-maximal inhibitory concentration
185 (IC_{50}) for each molecule when compared across the five species. *V. vulnificus* exhibits very low
186 IC_{50} values for all the top panel molecules (Fig. 4E), whereas *V. cholerae* is completely resistant
187 to these molecules even at high concentrations (Fig. 4B). Using 10B as an example, the IC_{50}
188 values are orders of magnitude different comparing *V. vulnificus* (0.002 μM) to *V. campbellii*
189 (0.35 μM) (Fig. 4A, 4E, Table S2). To further examine this observation, we assayed the top
190 panel of molecules against additional isolates for each species (Table S2). We observed that
191 the inhibitory effect of the molecules is similar for each isolate within a species (Table S2). For
192 example, the IC_{50} values for 10B for all three *V. vulnificus* isolates range from 2-30 nM. From
193 these data, we conclude that 10B has the highest inhibitory activity in all *Vibrio* species, with
194 variation in the IC_{50} that is specific to the *Vibrio* species tested.

195 We next focused on the best inhibitor in the panel, 10B, which is called 3-phenyl-1-
196 (thiophen-2-ylsulfonyl)-1*H*-pyrazole, and thus we will refer to it as PTSP from hereon. We
197 assessed LuxR function in the presence of PTSP by assaying protease production, a key
198 virulence activity in vibrios during pathogenesis and host cell lysis (Fig. 4F, 4G). LuxR proteins

activate several genes encoding proteases in *Vibrio* species, such as HapA in *V. cholerae*, VvpE in *V. vulnificus*, PrtA in *V. parahaemolyticus*, and VcpA/VcpB in *V. coralliilyticus* (previously called VtpA and VtpB when the strain was misidentified as *Vibrio tubiashii*)[23,40-43]. We analyzed protease activity of bacterial supernatants using azocasein as a substrate and compared wild-type strains to their isogenic Δ*luxR* counterparts for one representative strain for each species. In each species except *V. parahaemolyticus*, the wild-type strain produces significantly more protease activity than the Δ*luxR* strain (Fig. 4F). Addition of PTSP to the wild-type strain significantly reduces protease activity in *V. campbellii*, *V. coralliilyticus*, and *V. vulnificus*, but not in *V. cholerae* (Fig. 4F). *V. parahaemolyticus* exhibited extremely low protease activity in this assay, thus the effect of PTSP on *V. parahaemolyticus* cannot be ascertained in this experiment. We observed that the effect of PTSP on protease activity mirrors that of bioluminescence: PTSP has minimal activity against *V. coralliilyticus* and highest activity against *V. vulnificus*. (Fig. 4F). Although we assessed the effect of PTSP on protease activity in numerous strains for *V. campbellii*, *V. coralliilyticus*, and *V. parahaemolyticus*, the protease activity is so low in many of these isolates that an IC_{50} could not be reliably calculated for these (Fig. S4). However, for *V. vulnificus* strains, we calculated the IC_{50} values for PTSP inhibition and observed a similar range of protease inhibition as we observed for bioluminescence: ATCC 27562 = 6.8 nM, CMPC6 = 78.1 nM, and YJ016 = 18.3 nM (Fig. 4G). From the bioluminescence and protease assay data, we conclude that PTSP is a potent inhibitor of *V. vulnificus*, *V. parahaemolyticus*, and *V. campbellii*, with moderate effects on *V. coralliilyticus*. Inhibitor PTSP and derivatives are not active against *V. cholerae* (Fig. 4B, 4F, 4G). Further, we conclude that the use of the *E. coli* bioassay reporter is a valid assay for monitoring endogenous LuxR activity in these *Vibrio* species.

Mechanism of 2-thiophenesulfonamide efficacy

There are several possible reasons for the observed difference in PTSP inhibition in the various *Vibrio* species, including but not limited to: 1) differences in LuxR-inhibitor interaction(s), 2) differences in diffusion of the inhibitor across the membranes, or 3) stability of the inhibitor in the cell and/or cell culture. To examine PTSP activity in a common strain background, we cloned the *luxR* gene from each *Vibrio* species into a plasmid under control of an IPTG-inducible promoter and assayed the effect of PTSP against these proteins in the *E. coli* bioassay. We found that HapR is unresponsive to PTSP in *E. coli*, exhibiting a similar level of GFP expression to the negative control (Fig. 5B). Conversely, SmcR, LuxR, OpaR, and VcpR are each inhibited by PTSP with a trend similar to that observed in their native *Vibrio* cells, in which the order of sensitivity to PTSP inhibition is SmcR>LuxR>OpaR>VcpR (Fig. 5B). We conclude that the differences in PTSP activity in *Vibrio* species is due to differences in interaction between PTSP and the LuxR-type protein in each *Vibrio*.

Using the SmcR-Qstatin X-ray crystal structure as a guide[17], alignment of the LuxR-type proteins from each *Vibrio* species shows that there are four residues that interact with Qstatin in SmcR that are variable in HapR and/or VcpR (Fig. 5A). We therefore sought to determine if any of the four residues that differ between HapR and LuxR/SmcR in the putative ligand binding pocket are sufficient to render SmcR insensitive to PTSP. First, we introduced substitutions in SmcR to mimic the amino acid sequence of HapR: F75Y, I96L, V140I, and C170F. We observed that the substitutions of F75Y and C170F abolish PTSP inhibition, suggesting that F75 and C170 are both necessary for PTSP inhibition of SmcR transcription regulation *in vivo* (Fig. 5C). Next, we introduced single substitutions in HapR to mimic the amino acid present in SmcR: Y76F, L97I, I141V, and F171C. However, none of these substitutions alone are sufficient to make HapR sensitive to PTSP (Fig. 5C). From these results, we conclude that SmcR F75 and C170 are critical residues necessary for PTSP inhibition of SmcR activity.

Modeling of 2-thiophenesulfonamide inhibitors

Previous studies have used molecular docking simulations to predict effective inhibitors of LuxR family proteins[30]. To examine the accuracy of using molecular docking to predict effective inhibitors of LuxR proteins, we used Autodock Vina software[44] to simulate binding of molecules to the structure of SmcR and calculate the best binding mode and affinity (kcal/mol). First, to validate this modelling approach, we used Autodock Vina to predict the binding position of Qstatin into the SmcR (apo) X-ray crystal structure and compared it to the solved structure of SmcR-Qstatin (Fig. 6A). Although there is a slight shift (0.6 to 1.4 Å), the position and orientation of Qstatin within the putative ligand binding pocket of SmcR was accurately predicted by Autodock Vina (Fig. 6A). We next used Autodock Vina to predict the binding position of PTSP in both SmcR and HapR (Fig. 6B). We observed that PTSP is modeled in the opposite orientation in SmcR compared to HapR. This is likely driven at least partially by the rotational position of glutamine 137 in SmcR (Q138 in HapR) that clashes with the phenyl ring of PTSP. We also note that SmcR Q137 has multiple rotamers among the four SmcR chains within the asymmetric unit (Fig. 6C), and Autodock Vina modelling indicates that PTSP is oriented differently in SmcR chain A compared to chain B (Fig. 6D). Thus, the binding orientation and interactions of PTSP with SmcR are likely influenced, at least in part, by the orientation of Q137. For example, the predicted orientation of PTSP is different in chains A and B that have different Q137 rotamers and different predicted binding energies (Fig. S5; -7.5 kcal/mol for chain A compared to -0.2 kcal/mol for chain B). In addition, the predicted binding energies for PTSP in HapR are clearly worse at +1.6 kcal/mol for chain A and +10.4 kcal/mol for chain B (Fig. S5).

Because Autodock Vina accurately predicts the binding position of Qstatin in SmcR, we modelled binding of the top panel of molecules into SmcR. We plotted the predicted binding affinities for each molecule against the calculated IC_{50} values from the *in vivo* assay in *V. vulnificus* (Fig. 6E). Molecules 10A, 10B (PTSP), and 10C cluster with P0053 I18 in a group with the lowest predicted binding energies and lowest observed IC_{50} values (Fig. 6E). Conversely, the molecules with the low-moderate inhibitory activity were predicted to have similar binding

276 energies (Fig. 6E). However, these molecules group in two separate clusters, indicating that
277 modelling could not distinguish efficacy among low-moderate inhibitors. From these data, we
278 conclude that molecular docking simulations are an accurate method for predicting molecules
279 with good binding affinity and inhibitory activity against SmcR.

280 We note that Qstatin and PTSP are both predicted to bind in the putative ligand binding
281 pocket of SmcR. It is currently unknown how Qstatin allosterically affects DNA binding through
282 its interactions in the ligand binding domain. Kim *et al.* showed that Qstatin does not appreciably
283 alter the DNA binding constant for SmcR, but rather affects the entropy and enthalpy with which
284 it interacts with DNA[17]. We therefore also assessed the effect of sulfonamide PTSP on the DNA
285 binding activity of LuxR and SmcR *in vitro*. Addition of saturating concentrations of PTSP does
286 not alter DNA binding to LuxR or SmcR (Fig. 6F, Fig. S6). This result is similar to the finding that
287 Qstatin has very little effect on SmcR DNA binding affinity (Fig. 6F)[17]. Collectively, these data
288 show that thiophenesulfonamides inhibit the function of LuxR proteins to different levels. In
289 addition, these data suggest that the mechanism of inhibition by thiophenesulfonamides is likely
290 similar in both SmcR and LuxR.
291
292
293 **Discussion**

294 This study has aimed to test a panel of inhibitors against quorum sensing, a non-
295 essential cell signaling pathway that controls pathogenesis in *Vibrio* species. Using a previously
296 established dual-color bioassay, we screened thousands of compounds and synthesized a
297 broad panel to find potent inhibitors of the quorum sensing master transcription factor LuxR[8,22].
298 We observed that some of our key candidates contain sulfamide/sulfonamide heterocycles, but
299 there exists a vast range of inhibition between these various compounds. Using the best
300 candidate inhibitor PTSP, we tested its efficacy against five vibrios *in vivo* and found that it is
301 most effective towards *V. vulnificus*, followed by *V. campbellii, V. parahaemolyticus, V.*

coralliilyticus, and not effective against *V. cholerae.* The efficacy observed in inhibition of bioluminescence reporter assays was mimicked in protease assays where measurable. These results show that PTSP blocks all measured activities of LuxR proteins. This result is comparable to what was observed for the thiophenesulfonamide Qstatin, which blocks SmcR regulation of genes across the *V. vulnificus* genome to similar levels as a Δ*smcR* strain[17]. Thus, our results show that thiophenesulfonamides are broadly inhibitory of LuxR activities in multiple *Vibrio* species.

We were intrigued by the finding that the compounds we tested have no effect on HapR from *V. cholerae*. Our data show that HapR resistance is due to amino acid residue differences in the putative ligand binding pocket. We focused on differences in the residues in the Qstatin binding pocket across five *Vibrio* species, though substitution of single amino acids in HapR are not sufficient to render the protein sensitive to PTSP. We note that substitutions Y76F and F171C did not alter sensitivity to the PTSP molecule, but rather affected overall activity of HapR. We presume that multiple, combined substitutions in the HapR ligand binding pocket to change the sequence to match SmcR would likely result in HapR sensitivity to PTSP, though this needs to be formally tested. Interestingly, *V. cholerae* also has a very different pathogenic life cycle compared to other vibrios. Pathogenesis in the human host caused by *V. cholerae* occurs at LCD, where the bacterial cells attach to intestinal epithelial cells through the toxin co-regulated pilus and grow as a biofilm, producing cholera toxin. Growth of the population and accumulation of autoinducers drives inhibition of biofilms through various regulatory mechanisms, cleavage from the host epithelium by the HapA protease, and the cells are shed back into the marine environment[45-49]. This poses some intriguing evolutionary questions about *V. cholerae* pathogenesis and growth in the environment and the selective pressures that may have driven differences in amino acid conservation between HapR and other LuxR-family proteins. This could underscore the stark contrast in efficacy of inhibitors against HapR and other *Vibrio* LuxR-

type regulators that we observed in this study. We hypothesize that successful HapR inhibitors will require a more targeted approach.

Our modelling experiments successfully predicted the efficacy of the 10A, 10B (PTSP), and 10C molecules, which are the most potent LuxR inhibitors identified thus far. However, it is also clear that the modelling could not reliably predict every critical amino acid contact. Although we identified two critical residues in SmcR, F75 and C170, we hypothesize that more than one critical contact exists because these substitutions did not render HapR sensitive to PTSP. Although the structure of PTSP is similar to that of Qstatin, we were able to show that PTSP is >10X more inhibitory in our assays. We hypothesize that this molecule would make a better initial candidate for future experiments aimed at developing these molecules as therapeutics. In addition to our *in vivo* studies, our *in silico* studies allowed us to model binding affinities of compounds to accurately predict which compounds are best inhibitors of LuxR proteins. This tool will be very useful for future drug development as more compound classes are examined. While modeling has shown to be very effective in our experiments thus far, we recognize that a structure of PTSP bound to SmcR would provide the most information to further optimize *Vibrio* infection therapeutics for PTSP and derivatives.

Acknowledgements

We thank Stanna Dorn and the Indiana University students in Organic Chemistry C344 laboratory classes for synthesis of molecules in the thiophenesulfonamide panel. We thank the Indiana University School of Medicine Chemical Genomics Core Facility for assistance with chemical screens and analyses. We thank Dr. Irene Newton for assistance with data analysis.

Author Contributions

JVK and LCB designed the experiments, JVK, JDN, PS, JC, ES, MEM, and LCB performed experiments, JVK, JDN, RH, JC, ES, MEM, and LCB analyzed experimental results, and JVK, JDN, and LCB wrote the manuscript.

Competing Interests

The authors declare that they have no competing interests.

Funding

This work was supported by National Institutes of Health grant R35GM124698 to JVK and with support from the Indiana Clinical and Translational Sciences Institute funded, in part by Award Number UL1TR002529 from the National Institutes of Health, National Center for Advancing Translational Sciences, Clinical and Translational Sciences Award. The content is solely the responsibility of the authors and does not necessarily represent the official views of the National Institutes of Health.

References

1. Le Roux, F. et al. The emergence of Vibrio pathogens in Europe: ecology, evolution, and pathogenesis (Paris, 11-12th March 2015). *Front Microbiol* **6**, 830 (2015).
2. Newton, A., Kendall, M., Vugia, D.J., Henao, O.L. & Mahon, B.E. Increasing rates of vibriosis in the United States, 1996-2010: review of surveillance data from 2 systems. *Clin Infect Dis* **54 Suppl 5**, S391-5 (2012).
3. Vezzulli, L. et al. Climate influence on Vibrio and associated human diseases during the past half-century in the coastal North Atlantic. *Proc Natl Acad Sci U S A* **113**, E5062-71 (2016).
4. Girard, L. Quorum sensing in Vibrio spp.: the complexity of multiple signalling molecules in marine and aquatic environments. *Crit Rev Microbiol* **45**, 451-471 (2019).
5. Rutherford, S.T. & Bassler, B.L. Bacterial quorum sensing: its role in virulence and possibilities for its control. *Cold Spring Harb Perspect Med* **2**(2012).

6. Ball, A.S. & van Kessel, J.C. The master quorum-sensing regulators LuxR/HapR directly interact with the alpha subunit of RNA polymerase to drive transcription activation in Vibrio harveyi and Vibrio cholerae. *Mol Microbiol* **111**, 1317-1334 (2019).
7. Ng, W.L. & Bassler, B.L. Bacterial quorum-sensing network architectures. *Annu Rev Genet* **43**, 197-222 (2009).
8. van Kessel, J.C., Rutherford, S.T., Shao, Y., Utria, A.F. & Bassler, B.L. Individual and combined roles of the master regulators AphA and LuxR in control of the Vibrio harveyi quorum-sensing regulon. *J Bacteriol* **195**, 436-43 (2013).
9. Rutherford, S.T., van Kessel, J.C., Shao, Y. & Bassler, B.L. AphA and LuxR/HapR reciprocally control quorum sensing in vibrios. *Genes Dev* **25**, 397-408 (2011).
10. Kernell Burke, A. et al. OpaR controls a network of downstream transcription factors in Vibrio parahaemolyticus BB22OP. *PLoS One* **10**, e0121863 (2015).
11. Kim, S.M. et al. LuxR homologue SmcR is essential for Vibrio vulnificus pathogenesis and biofilm detachment, and its expression is induced by host cells. *Infect Immun* **81**, 3721-30 (2013).
12. Lee, D.H. et al. A consensus sequence for binding of SmcR, a Vibrio vulnificus LuxR homologue, and genome-wide identification of the SmcR regulon. *J Biol Chem* **283**, 23610-8 (2008).
13. Tsou, A.M., Cai, T., Liu, Z., Zhu, J. & Kulkarni, R.V. Regulatory targets of quorum sensing in Vibrio cholerae: evidence for two distinct HapR-binding motifs. *Nucleic Acids Res* **37**, 2747-56 (2009).
14. Ball, A.S., Chaparian, R.R. & van Kessel, J.C. Quorum Sensing Gene Regulation by LuxR/HapR Master Regulators in Vibrios. *J Bacteriol* **199**(2017).
15. Fuqua, W.C., Winans, S.C. & Greenberg, E.P. Quorum sensing in bacteria: the LuxR-LuxI family of cell density-responsive transcriptional regulators. *J Bacteriol* **176**, 269-75 (1994).
16. Ramos, J.L. et al. The TetR family of transcriptional repressors. *Microbiol Mol Biol Rev* **69**, 326-56 (2005).
17. Kim, B.S. et al. QStatin, a Selective Inhibitor of Quorum Sensing in Vibrio Species. *MBio* **9**(2018).
18. Kim, Y. et al. Crystal structure of SmcR, a quorum-sensing master regulator of Vibrio vulnificus, provides insight into its regulation of transcription. *J Biol Chem* **285**, 14020-30 (2010).
19. De Silva, R.S. et al. Crystal structure of the Vibrio cholerae quorum-sensing regulatory protein HapR. *J Bacteriol* **189**, 5683-91 (2007).
20. Chaparian, R.R., Olney, S.G., Hustmyer, C.M., Rowe-Magnus, D.A. & van Kessel, J.C. Integration host factor and LuxR synergistically bind DNA to coactivate quorum-sensing genes in Vibrio harveyi. *Mol Microbiol* **101**, 823-40 (2016).
21. Chaparian, R.R., Tran, M.L.N., Miller Conrad, L.C., Rusch, D.B. & van Kessel, J.C. Global H-NS counter-silencing by LuxR activates quorum sensing gene expression. *Nucleic Acids Res* **48**, 171-183 (2020).
22. van Kessel, J.C., Ulrich, L.E., Zhulin, I.B. & Bassler, B.L. Analysis of activator and repressor functions reveals the requirements for transcriptional control by LuxR, the master regulator of quorum sensing in Vibrio harveyi. *mBio* **4**(2013).

23. Hasegawa, H. & Hase, C.C. TetR-type transcriptional regulator VtpR functions as a global regulator in Vibrio tubiashii. *Appl Environ Microbiol* **75**, 7602-9 (2009).
24. Remy, B. et al. Interference in Bacterial Quorum Sensing: A Biopharmaceutical Perspective. *Front Pharmacol* **9**, 203 (2018).
25. Jiang, Q., Chen, J., Yang, C., Yin, Y. & Yao, K. Quorum Sensing: A Prospective Therapeutic Target for Bacterial Diseases. *Biomed Res Int* **2019**, 2015978 (2019).
26. Starkey, M. et al. Identification of anti-virulence compounds that disrupt quorum-sensing regulated acute and persistent pathogenicity. *PLoS Pathog* **10**, e1004321 (2014).
27. Guendouze, A. et al. Effect of Quorum Quenching Lactonase in Clinical Isolates of Pseudomonas aeruginosa and Comparison with Quorum Sensing Inhibitors. *Front Microbiol* **8**, 227 (2017).
28. Brackman, G. et al. Structure-activity relationship of cinnamaldehyde analogs as inhibitors of AI-2 based quorum sensing and their effect on virulence of Vibrio spp. *PLoS ONE* **6**, e16084 (2011).
29. Defoirdt, T. et al. A quorum sensing-disrupting brominated thiophenone with a promising therapeutic potential to treat luminescent vibriosis. *PLoS ONE* **7**, e41788 (2012).
30. Rajamanikandan, S., Jeyakanthan, J. & Srinivasan, P. Discovery of potent inhibitors targeting Vibrio harveyi LuxR through shape and e-pharmacophore based virtual screening and its biological evaluation. *Microb Pathog* **103**, 40-56 (2017).
31. Rajamanikandan, S., Jeyaraman, J. & Pappu, S. Binding mode exploration of LuxR-thiazolidinedione analogues, e-pharmacophore based virtual screening in the designing of LuxR inhibitors and its biological evaluation. *J Biomol Struct Dyn*, 1-57 (2016).
32. Defoirdt, T. et al. The natural furanone (5Z)-4-bromo-5-(bromomethylene)-3-butyl-2(5H)-furanone disrupts quorum sensing-regulated gene expression in Vibrio harveyi by decreasing the DNA-binding activity of the transcriptional regulator protein luxR. *Environ Microbiol* **9**, 2486-95 (2007).
33. Kim, S.M. et al. Phenotypic Discovery of an Antivirulence Agent against Vibrio vulnificus via Modulation of Quorum-Sensing Regulator SmcR. *ACS Infect Dis* (2020).
34. Hammoudeh, D.I., Zhao, Y., White, S.W. & Lee, R.E. Replacing sulfa drugs with novel DHPS inhibitors. *Future Med Chem* **5**, 1331-40 (2013).
35. Roland, S., Ferone, R., Harvey, R.J., Styles, V.L. & Morrison, R.W. The characteristics and significance of sulfonamides as substrates for Escherichia coli dihydropteroate synthase. *J Biol Chem* **254**, 10337-45 (1979).
36. Jung, S.A., Hawver, L.A. & Ng, W.L. Parallel quorum sensing signaling pathways in Vibrio cholerae. *Curr Genet* **62**, 255-60 (2016).
37. Lenz, D.H., Miller, M.B., Zhu, J., Kulkarni, R.V. & Bassler, B.L. CsrA and three redundant small RNAs regulate quorum sensing in Vibrio cholerae. *Mol Microbiol* **58**, 1186-202 (2005).
38. Miller, M.B., Skorupski, K., Lenz, D.H., Taylor, R.K. & Bassler, B.L. Parallel quorum sensing systems converge to regulate virulence in Vibrio cholerae. *Cell* **110**, 303-14 (2002).
39. Simpson, C.A., Podicheti, R., Rusch, D.B., Dalia, A.B. & van Kessel, J.C. Diversity in Natural Transformation Frequencies and Regulation across Vibrio Species. *mBio* **10**(2019).

40. Jeong, H.S., Lee, M.H., Lee, K.H., Park, S.J. & Choi, S.H. SmcR and cyclic AMP receptor protein coactivate Vibrio vulnificus vvpE encoding elastase through the RpoS-dependent promoter in a synergistic manner. *J Biol Chem* **278**, 45072-81 (2003).
41. Jobling, M.G. & Holmes, R.K. Characterization of hapR, a positive regulator of the Vibrio cholerae HA/protease gene hap, and its identification as a functional homologue of the Vibrio harveyi luxR gene. *Mol Microbiol* **26**, 1023-34 (1997).
42. Chang, S.C. & Lee, C.Y. OpaR and RpoS are positive regulators of a virulence factor PrtA in Vibrio parahaemolyticus. *Microbiology (Reading)* **164**, 221-231 (2018).
43. Shinoda, S. & Miyoshi, S. Proteases produced by vibrios. *Biocontrol Sci* **16**, 1-11 (2011).
44. Trott, O. & Olson, A.J. AutoDock Vina: improving the speed and accuracy of docking with a new scoring function, efficient optimization, and multithreading. *J Comput Chem* **31**, 455-61 (2010).
45. Hammer, B.K. & Bassler, B.L. Quorum sensing controls biofilm formation in Vibrio cholerae. *Mol Microbiol* **50**, 101-4 (2003).
46. Vance, R.E., Zhu, J. & Mekalanos, J.J. A constitutively active variant of the quorum-sensing regulator LuxO affects protease production and biofilm formation in Vibrio cholerae. *Infect Immun* **71**, 2571-6 (2003).
47. Waters, C.M., Lu, W., Rabinowitz, J.D. & Bassler, B.L. Quorum sensing controls biofilm formation in Vibrio cholerae through modulation of cyclic di-GMP levels and repression of vpsT. *J Bacteriol* **190**, 2527-36 (2008).
48. Zhu, J. & Mekalanos, J.J. Quorum sensing-dependent biofilms enhance colonization in Vibrio cholerae. *Dev Cell* **5**, 647-56 (2003).
49. Papenfort, K. et al. A Vibrio cholerae autoinducer-receptor pair that controls biofilm formation. *Nat Chem Biol* **13**, 551-557 (2017).

Figure Legends

Figure 1. The quorum sensing pathway in *Vibrio* species. Autoinducer molecules are bound by membrane-bound histidine kinase receptors, which alters the phosphorylation cascade downstream. At high cell densities, the production of the transcription factor LuxR is maximal, and LuxR activates and represses genes encoding proteins with various functions, some of which are listed in the diagram. LuxR protein homologs in various *Vibrio* species are listed.

Figure 2. Screen for LuxR inhibitors in *E. coli* bioassay. (A) Diagram of the two plasmids in the *E. coli* bioassay used to screen for LuxR inhibitors. Plasmid 1 (pJV064) contains divergent promoters for *V. campbellii luxCDABE* and *05222* driving expression of *gfp* and *mCherry*, respectively. Plasmid 2 (pKM699) contains the *V. campbellii luxR* gene under control of its native promoter. (B) Fluorescence expression (GFP/OD_{600} or $mCherry/OD_{600}$) in *E. coli* bioassay cells (with pJV064) expressing LuxR (pKM699) or the empty vector control (pLAFR2). (C) Structures of LuxR inhibitors identified and verified from the compound library screen. (D, E) Production of GFP (panel D; GFP/OD_{600}) or mCherry (panel E; $mCherry/OD_{600}$) in the presence of LuxR inhibitors titrated into the *E. coli* bioassay strain (pKM699, pJV064). DMSO was titrated as a solvent control with an equal volume to the 100 μM concentration of compound and compared to cells in which nothing was added (-, plotted at 100 μM point on x-axis). Data shown represent the mean and standard deviation of at least three biological replicates.

Figure 3. Panel of thiophenesulfonamide molecules that inhibit LuxR. Substrates with modifications to the heteroaromatic ring (pyrazole in the case of Qstatin) have number designations, and substrates with modifications to the thiophene ring have letter designations. (B, C) Production of GFP (panel B; GFP/OD_{600}) or mCherry (panel C; $mCherry/OD_{600}$) in the presence of thiophenesulfonamide compounds titrated into the *E. coli* bioassay strain (pKM699, pJV064). DMSO was titrated as a solvent control with an equal volume to the 100 μM concentration of compound and compared to cells in which nothing was added (-, plotted at 100 μM point on x-axis). Data shown represent the mean and standard deviation of at least three biological replicates.

Figure 4. Thiophenesulfonamides have a range of inhibition against *Vibrio* species. (A-E) Titration of molecules from the top panel of thiophenesulfonamides in *Vibrio* strains compared to

DMSO solvent control (DMSO was titrated with an equal volume to the 100 μM concentration of compound). Data shown represent the mean and standard deviation of three biological replicates. (F) Protease activity (final assay OD_{420}/initial culture OD_{600}) for wild-type and mutant *Vibrio* strains in the presence of 2.5 μM PTSP or an equal volume of the DMSO solvent. Asterisks indicate significant differences (two-way analysis of variance (ANOVA) followed by Sidak's multiple comparisons test, $n = 4$; *, $p = 0.05$; **, $p = 0.01$; ***, $p = 0.001$; ****, $p = 0.0001$; ns, not significant). (G) Protease activity (final assay OD_{420}/initial culture OD_{600}) for *Vibrio* strains in the presence of PTSP titrated into the cultures. Data shown represent the mean and standard deviation of three biological replicates.

Figure 5. Sulfonamide 10B does not inhibit *V. cholerae* HapR. (A) LuxR sequences from *V. coralliilyticus* OCN008 (accession: ERB64458.1), *V. campbellii* BB120 (accession: ABU72404.1), *V. vulnificus* ATCC 27562 (accession: WP_011079558.1), *V. parahaemolyticus* RIMD 2210633 (accession: WP_005479697.1), and *V. cholerae* C6706 (accession: ACB30340.1) aligned using Clustal Omega and Boxshade. Blue dots indicate the amino acids in SmcR that contact Qstatin in the published SmcR-Qstatin X-ray crystal structure[17]. Green dots indicate amino acid differences between LuxR proteins in each species among the SmcR-Qstatin contacts. (B) Production of GFP (GFP/OD_{600}) in the presence of 25 μM PTSP or DMSO solvent control in the *E. coli* bioassay strain (pJV064) containing plasmids expressing SmcR (pJN22), HapR (pJV387), LuxR (pJV388), OpaR (pJV389), VcpR (pJV390), or empty vector (pMMB67EH-kanR). SmcR and HapR expression in strains was induced with 50 μM IPTG; IPTG was not added to cultures of the remaining strains. (C) Production of GFP (GFP/OD_{600}) in the presence of 25 μM PTSP or DMSO solvent control in the *E. coli* bioassay strain (pJV064) containing plasmids expressing SmcR (pJN22), HapR (pJV387), or the listed various amino acid substitution mutants. SmcR and HapR expression was induced with 50 μM IPTG. For panels B

552 and C, asterisks indicate significant differences (two-way ANOVA followed by Sidak's multiple
553 comparisons test, n = 3 (panel B), n = 6 (panel C); ****, p = 0.0001; ns, not significant).
554
555 **Figure 6.** (A) Autodock Vina modelling of Qstatin into the SmcR apo X-ray crystal structure
556 (3KZ9; cyan) overlaid with the X-ray structure of SmcR complexed with Qstatin (5X3R; green).
557 (B) Autodock Vina modelling of PTSP (10B) in the X-ray crystal structures of SmcR (3KZ9;
558 cyan) and HapR (2PBX; gray). (C) The rotational orientation of Q137 in the four chains of SmcR
559 from the asymmetric unit (3KZ9). (D) Autodock Vina modelling of PTSP into chain A (left) and
560 chain B (right) of SmcR (3KZ9). (E) Binding affinities predicted by Autodock Vina for each
561 molecule modelled into the SmcR X-ray crystal structure (3KZ9) are graphed against the IC_{50}
562 value for each molecule determined by assaying bioluminescence production in *V. vulnificus*
563 ATCC27562 (Table S2). Clusters of the 4 (blue), 6 (red), and 3 (green) data points were
564 generated using K-means clustering analysis in R. (F) Electrophoretic mobility shift assays
565 (EMSAs) of SmcR purified protein in varying concentrations incubated with radiolabeled dsDNA
566 corresponding to the *V. vulnificus vvpE* promoter. DNA shifts were quantified using ImageJ, and
567 the graphs show the mean and standard deviation for three biological replicates.
568
569
570

Thiophenesulfonamides are specific inhibitors of quorum sensing in pathogenic Vibrios

Jane D. Newman, Priyanka Shah, Jay Chopra, Eda Shi, Molly E. McFadden, Rachel E. Horness, Laura C. Brown, Julia C. van Kessel

Methods

Bacterial strains and media

All strains used in this study are listed in Table S3. *E. coli* strains DH10B and S17-1λpir were used for cloning, and BL21(DE3) was used for overexpression of LuxR and SmcR proteins. All *E. coli* strains, *V. cholerae* strains, and derivatives were grown in Lysogeny Broth (LB) at 30°C shaking at 275 RPM in LB media with the appropriate antibiotic. *V. campbellii*, *V. parahaemolyticus*, *V. coralliilyticus*, and *V. vulnificus* strains and derivatives were grown shaking at 275 RPM at 30°C in Luria Marine (LM) medium (LB with 2% NaCl) with appropriate antibiotics. Antibiotics were used at the following concentrations: kanamycin 50 μg/mL or 250 μg/mL (*E. coli* or *Vibrio*, respectively), chloramphenicol 10 μg/mL, ampicillin 100 μg/mL, gentamicin 100 μg/mL, and tetracycline 10 μg/mL.

Molecular methods

All PCR reactions were performed using Phusion HF polymerase (NEB). T4 polynucleotide kinase (T4 PNK) used in EMSAs and all other enzymes were purchased from NEB and used according to manufacturer's instructions. Site-directed mutagenesis for construction of plasmids expressing mutant proteins was carried out using the Agilent QuikChange II XL Site-Directed Mutagenesis Kit. All oligonucleotides were purchased from Integrated DNA Technologies (IDT), and those used in this study are listed (Table S4). All

plasmid constructs (Table S5) were confirmed by DNA sequencing (Eurofins). Cloning details for plasmids are available upon request.

Compound synthesis and purchase

Synthesis and characterization data for 1B-C, 3A-C, 8A-C, 10A-C, P007 H4, P2065 E16, and P2065 E16-CF_3 are provided in the supplementary methods. Compounds P0053 O05 and P1117 F20 were purchased from Lab Network, P1120 D05 and P0074 N08 were purchased from EnamineStore, and P0053 I18 was purchased from ChemDiv.

E. coli *bioassay*

The dual promoter fluorescence reporter assays were performed using *E. coli* strain DH10B containing two plasmids: 1) plasmid pJV064 containing the P_{luxC} fused to GFP and P_{05222} fused to mCherry to assess LuxR transcriptional regulation[1], and 2) plasmid pKM699 expressing *V. campbellii luxR* under control of its native promoter or empty vector pLAFR2[2]. Overnight *E. coli* cultures containing either pKM699 or pLAFR2 and the pJV064 reporter were diluted 1:100 into LB with chloramphenicol and tetracycline and aliquoted into black-welled, clear-bottomed 96-well plates (150 μl final volume). Compounds were resuspended in DMSO and added to *E. coli* cultures at varying concentrations, or DMSO was added as a negative control at equal volumes. 96-well plates were covered in microporous sealing tape and grown for 16 hours shaking at 275 RPM at 30°C. The OD_{600} and fluorescence (both GFP and mCherry) were measured on a BioTek Cytation plate reader.

Protein purification and electrophoretic mobility shift assays (EMSAs)

SmcR and LuxR were purified as described previously[3]. EMSAs were conducted as described previously[3,4] using oligonucleotides corresponding to the *luxC* and *vvpE* promoter sequences (Table S4).

53

54 *Assaying compounds in* Vibrio *cultures*

55 *Vibrio* strains were inoculated in 5 ml LM (or LB for *V. cholerae*) overnight at 30°C
56 shaking at 275 RPM with kanamycin (100 μg/ml) or gentamicin (15 μg/ml) to select for the
57 P*luxC-gfp* reporter plasmids pCS19 or pCS42, respectively. Cultures were back-diluted 1:1,000
58 in LB or LM with antibiotics, and the cell mixture was aliquoted into black-welled, clear-bottomed
59 96-well plates. Compounds were titrated into the wells (4-fold dilution series; final volume of 150
60 μl). DMSO was added as a negative control at equal volumes into control reactions. 96-well
61 plates were covered in microporous sealing tape and grown for 16 hours shaking at 275 RPM at
62 30°C. The OD_{600} and GFP fluorescence or bioluminescence were measured on a BioTek
63 Cytation plate reader.

64

65 *Protease assays*

66 *Vibrio* strains were inoculated in 5 ml LM (or LB for *V. cholerae*) overnight at 30°C
67 shaking at 275 RPM. Cultures were back-diluted 1:1,000 in LB or LM, and the cell mixture was
68 aliquoted into black-welled, clear-bottomed 96-well plates. Compounds were either added into
69 the wells to a specific final concentration or a titration series was performed (4-fold dilution
70 series; final volume of 150 μl; 3 technical replicates per sample). DMSO was added as a
71 negative control at equal volumes into control reactions. 96-well plates were covered in
72 microporous sealing tape and grown for 16 hours shaking at 275 RPM at 30°C. After incubation,
73 the OD_{600} was measured on a BioTek Cytation plate reader. The cultures were pelleted in the
74 96-well plate by centrifuging at 3700 RPM for 5 min at room temperature. 20 μl of the
75 supernatant was transferred to a new clear 96-well plate. 80 μl of 1% azocasein (dissolved in
76 dH_2O) was added to the supernatants and incubated at 37°C for 30 min. 120 μl of 10%
77 trichloracetic acid was added to the reaction, and the plate was incubated on ice for 30 min,

78 then centrifuged at 3700 RPM for 5 min at room temperature. 80 μl of the protease reaction was
79 transferred to a new clear 96-well plate, and 20 μl of 1.8N NaOH was added. The OD_{420} was
80 measured on a BioTek Cytation plate reader. Protease activity was calculated by dividing OD_{420}
81 by OD_{600}. Each assay was performed in biological triplicates.
82
83 *Autodock Vina modeling and analyses*
84 All docking experiments were performed using Autodock Vina[5]. Xray crystal structures
85 of apo SmcR (PDB ID 3KZ9) and HapR (PDB ID 2PBX) were used for all simulations[6,7].
86 Structures were prepared for docking using AutoDockTools-1.5.6 for addition of hydrogen atoms
87 and assignment of partial charge[8]. Ligand structures were similarly prepared to include using
88 AutoDockTools which was additionally used to define torsional degrees of freedom. An
89 approximately 14 x 14 x 14 Å box was defined surrounding the residues previously reported to
90 form the Qstatin binding site (box size varied slightly with protein)[9]. Pymol was used visualize
91 the lowest energy solutions. The predicted binding affinities from AutoDock Vina modeling were
92 analyzed compared to the observed IC50 values using K-means clustering in R using 3 clusters
93 of sizes 3, 6, and 4.
94
95 *Synthesis of LuxR Inhibitors:*
96
97 **General Methods:** ^{1}H NMR spectra were recorded at room temperature on a Varian I400 (400
98 MHz) or Varian VXR400 (400 MHz) spectrometer. Chemical shifts are reported in ppm from
99 tetramethylsilane with the residual solvent resonance as the internal standard (CHCl3: δ 7.26
100 ppm). Data are reported as follows: chemical shift, multiplicity (s = singlet, d = doublet, t = triplet,
101 q = quartet, br = broad, m = multiplet), coupling constants (Hz), and integration. ^{13}C NMR
102 spectra were recorded on a Varian I400 (100 MHz) or Varian VXR400 (100 MHz) spectrometer

with complete proton decoupling. Chemical shifts are reported in ppm from tetramethylsilane with the solvent resonance as the internal standard (CDCl3: δ 77.16 ppm). High Resolution Mass Spectrometry (HRMS) analysis was obtained using Electron Impact Ionization (EI), Chemical Ionization (CI), Atmospheric Pressure Chemical Ionization (APCI) or Electrospray Ionization (ESI) and reported as m/z (relative intensity). ESI was acquired using a Waters/Micromass LCT Classic (ESI-TOF). Dichloromethane (DCM) and tetrahydrofuran (THF) were purified under a positive pressure of dry argon by passage through two columns of activated alumina. Triethylamine (Et_3N) and diisopropylethylamine (DIPEA) were distilled over CaH_2. All other reagents and solvents were used without purification. All work-up and purification procedures were carried out with reagent grade solvents (purchased from Sigma-Aldrich) in air. Thin-layer chromatography (TLC) was performed on Merck Silica Gel 60 F254 glass plates and visualized with UV and/or standard potassium permanganate, phosphomolybdic acid staining techniques. Standard column chromatography techniques using ZEOprep 60/40-63 µm silica gel was used for purification.

General procedure for synthesis of inhibitors 1, 3, 8, 10:[10]

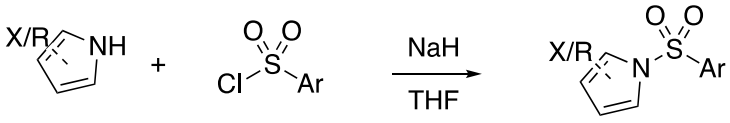

To a solution of amine (6 mmol) in tetrahydrofuran (15 mL) was added sodium hydride (60% in oil, 320 mg, 8 mmol) at room temperature, and the mixture was allowed to stir for 10 min. A solution of sulfonyl chloride (4 mmol) in tetrahydrofuran (5 mL) was added, and the mixture was allowed to stir for an additional 30 min. The reaction mixture was diluted with 20 mL water, and extracted with ethyl acetate (3 x 20 mL). The extract was washed with 20 mL saturated NaCl (brine), dried over anhydrous magnesium sulfate, and concentrated under reduced pressure.

The resulting crude product mixture was purified via SiO_2 column chromatography in 10:1 Hexanes:EtOAc to give the desired product.

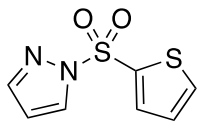

1B

1-(thiophen-2-ylsulfonyl)-1*H*-pyrazole (**1B**): **^{1}H NMR (400 MHz, $CDCl_3$)**: δ 8.08 (d, *J* = 2.7 Hz, 1H), 7.82 (dd, *J* = 3.9, 1.4 Hz, 1H), 7.74 (d, *J* = 1.6 Hz, 1H), 7.71 (dd, *J* = 5.0, 1.4 Hz, 1H), 7.09 (dd, *J* = 5.0, 3.9 Hz, 1H), 6.39 (dd, *J* = 2.8, 1.6 Hz, 1H). **^{13}C NMR (101 MHz, $CDCl_3$):** δ 145.44, 136.73, 135.51, 135.49, 131.08, 127.87, 109.07. **HRMS (ESI):** Calculated for $C_7H_6O_2N_2NaS_2$ [M+Na^+]: 236.9763. Found: 236.9763.

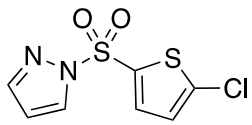

1C

1-((5-chlorothiophen-2-yl)sulfonyl)-1*H*-pyrazole (**1C**): **^{1}H NMR (400 MHz, $CDCl_3$)**: δ 8.06 (d, *J* = 2.8 Hz, 1H), 7.77 (d, *J* = 1.6 Hz, 1H), 7.64 (d, *J* = 4.2 Hz, 1H), 6.94 (d, *J* = 4.2 Hz, 1H), 6.42 (dd, *J* = 2.8, 1.6 Hz, 1H). **^{13}C NMR (101 MHz, $CDCl_3$):** (101 MHz, cdcl$_3$) δ 145.69, 141.32, 134.99, 134.33, 131.10, 127.22, 109.27. **HRMS (APCI):** Calculated for $C_7H_6ClN_2O_2S_2$ [M+H^+]: 248.9554. Found: 248.9554.

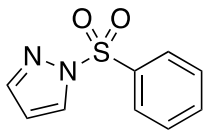

1E

1-(phenylsulfonyl)-1*H*-pyrazole (**1E**): **^{1}H NMR (400 MHz, $CDCl_3$)**: δ 8.10 (d, *J* = 2.8 Hz, 1H), 8.03 – 7.95 (m, 2H), 7.71 (d, *J* = 1.6 Hz, 1H), 7.66 – 7.57 (m, 1H), 7.56 – 7.46 (m, 2H), 6.38 (dd, *J* =

2.8, 1.6 Hz, 1H). **^{13}C NMR (101 MHz, $CDCl_3$):** δ 145.37, 137.05, 134.55, 131.24, 129.39, 128.03, 108.91. **HRMS (ESI):** Calculated for $C_9H_8O_2N_2NaS$ [$M+Na^+$]: 231.0199. Found: 231.0199.

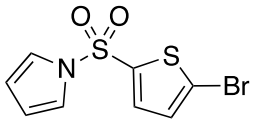

3A

1-((5-bromothiophen-2-yl)sulfonyl)-1*H*-pyrrole (**3A**): **^{1}H NMR (400 MHz, $CDCl_3$):** δ 7.40 (d, *J* = 4.1 Hz, 1H), 7.13 (t, *J* = 2.3 Hz, 2H), 7.02 (d, *J* = 4.1 Hz, 1H), 6.32 (t, *J* = 2.3 Hz, 2H). **^{13}C NMR (101 MHz, $CDCl_3$):** δ 139.87, 133.46, 130.52, 122.26, 120.72, 114.31. **HRMS (APCI):** Calculated for $C_8H_7O_2NBrS_2$ [$M+H^+$]: 291.9096. Found: 291.9098

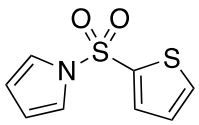

3B

1-(thiophen-2-ylsulfonyl)-1*H*-pyrrole (**3B**): **^{1}H NMR (400 MHz, $CDCl_3$):** δ 7.63 (ddd, *J* = 13.5, 4.4, 1.4 Hz, 2H), 7.17 (t, *J* = 2.3 Hz, 2H), 7.04 (dd, *J* = 5.1, 3.8 Hz, 1H), 6.30 (t, *J* = 2.3 Hz, 2H). **^{13}C NMR (101 MHz, $CDCl_3$):** δ 139.39, 133.80, 133.37, 127.54, 120.74, 113.90. **HRMS (EI):** Calculated for $C_8H_7NO_2S_2$ [M^+]: 212.9913. Found: 212.9916.

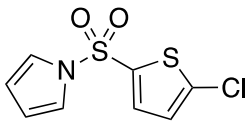

3C

1-((5-chlorothiophen-2-yl)sulfonyl)-1*H*-pyrrole (**3C**): **^{1}H NMR (400 MHz, $CDCl_3$):** δ 7.44 (d, *J* = 4.1 Hz, 1H), 7.14 (t, *J* = 2.3 Hz, 2H), 6.87 (d, *J* = 4.1 Hz, 1H), 6.32 (t, *J* = 2.3 Hz, 2H). **^{13}C NMR**

(101 MHz, $CDCl_3$): δ 139.51, 136.99, 132.88, 126.99, 120.73, 114.34. **HRMS (EI):** Calculated for $C_8H_6O_2NClS_2$ [M^+]: 246.9528. Found: 246.9533.

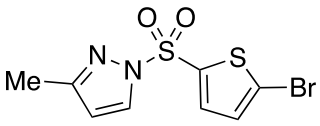

8A

1-((5-bromothiophen-2-yl)sulfonyl)-3-methyl-1*H*-pyrazole (**8A**): **^{1}H NMR (400 MHz, $CDCl_3$):** δ 7.92 (d, *J* = 2.7 Hz, 1H), 7.55 (d, *J* = 4.1 Hz, 1H), 7.05 (d, *J* = 4.1 Hz, 1H), 6.21 (d, *J* = 2.7 Hz, 1H), 2.28 (s, 3H). **^{13}C NMR (101 MHz, $CDCl_3$):** δ 156.08, 137.68, 135.16, 132.02, 130.69, 123.51, 110.25, 14.01. **HRMS (ESI):** Calculated for $C_8H_7O_2N_2BrNaS_2$ [M+Na^+]: 330.9003. Found: 330.9004.

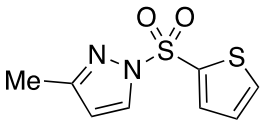

8B

3-methyl-1-(thiophen-2-ylsulfonyl)-1*H*-pyrazole (**8B**): **^{1}H NMR (400 MHz, $CDCl_3$):** δ 7.96 (d, *J* = 2.7 Hz, 1H), 7.80 (dd, *J* = 3.9, 1.4 Hz, 1H), 7.68 (dd, *J* = 5.0, 1.4 Hz, 1H), 7.08 (dd, *J* = 5.0, 3.8 Hz, 1H), 6.20 (d, *J* = 2.7 Hz, 1H), 2.27 (s, 3H). **^{13}C NMR (101 MHz, $CDCl_3$):** δ 155.70, 137.22, 135.06, 134.93, 131.99, 127.71, 109.96, 13.98. **HRMS (ESI):** Calculated for $C_8H_8N_2O_2S_2Na$ [M+Na^+]: 250.9919. Found: 250.9920.

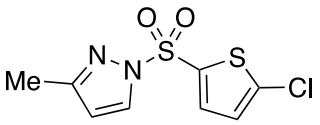

8C

1-((5-chlorothiophen-2-yl)sulfonyl)-3-methyl-1*H*-pyrazole (**8C**): **^{1}H NMR (400 MHz, $CDCl_3$):** δ 7.92 (d, *J* = 2.7 Hz, 1H), 7.59 (d, *J* = 4.2 Hz, 1H), 6.91 (d, *J* = 4.1 Hz, 1H), 6.21 (d, *J* = 2.8 Hz,

1H), 2.28 (s, 3H). **^{13}C NMR (101 MHz, $CDCl_3$):** δ 156.08, 140.71, 134.79, 134.54, 132.02, 127.10, 110.25, 14.00. **HRMS (ESI):** Calculated for $C_8H_7O_2N_2ClNaS_2$ [M+Na^+]: 283.9530. Found: 284.9531.

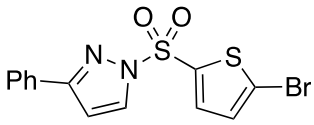

10A

1-((5-bromothiophen-2-yl)sulfonyl)-3-phenyl-1*H*-pyrazole (**10A**): **^{1}H NMR (400 MHz, $CDCl_3$):** δ 8.08 (d, *J* = 2.8 Hz, 1H), 7.87 – 7.79 (m, 2H), 7.61 (d, *J* = 4.1 Hz, 1H), 7.45 – 7.37 (m, 3H), 7.05 (d, *J* = 4.1 Hz, 1H), 6.73 (d, *J* = 2.8 Hz, 1H). **^{13}C NMR (101 MHz, $CDCl_3$):** δ 157.47, 137.37, 135.42, 132.53, 131.12, 130.73, 129.48, 128.74, 126.49, 123.94, 107.10. **HRMS (ESI):** Calculated for $C_{13}H_9BrN_2O_2S_2Na$ [M+Na^+]: 390.9181. Found: 390.9182

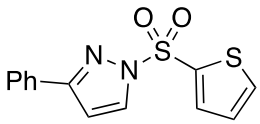

10B

3-phenyl-1-(thiophen-2-ylsulfonyl)-1*H*-pyrazole (**10B**): **^{1}H NMR (400 MHz, $CDCl_3$):** δ 8.11 (d, *J* = 2.8 Hz, 1H), 7.88 – 7.79 (m, 3H), 7.68 (dd, *J* = 5.0, 1.4 Hz, 1H), 7.44 – 7.31 (m, 3H), 7.07 (dd, *J* = 5.0, 3.9 Hz, 1H), 6.71 (d, *J* = 2.8 Hz, 1H). **^{13}C NMR (101 MHz, $CDCl_3$):** δ 157.17, 136.84, 135.40, 135.36, 132.55, 131.28, 129.36, 128.72, 127.79, 126.47, 106.90. **HRMS (ESI):** Calculated for $C_{13}H_{10}O_2N_2NaS_2$ [M+Na^+]: 313.0076. Found: 313.0078.

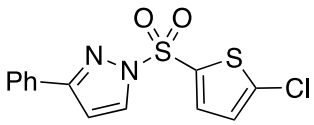

10C

1-((5-chlorothiophen-2-yl)sulfonyl)-3-phenyl-1*H*-pyrazole (**10C**): **^{1}H NMR (400 MHz, $CDCl_3$):** δ 8.08 (d, *J* = 2.8 Hz, 1H), 7.87 – 7.79 (m, 2H), 7.65 (d, *J* = 4.2 Hz, 1H), 7.41 (s, 1H), 7.43 – 7.33 (m, 2H), 6.92 (d, *J* = 4.1 Hz, 1H), 6.73 (d, *J* = 2.8 Hz, 1H). **^{13}C NMR (101 MHz, $CDCl_3$):** δ 157.47, 141.13, 134.79, 134.50, 132.51, 131.12, 129.47, 128.74, 127.12, 126.48, 107.08. **HRMS (ESI):** Calculated for $C_{13}H_9O_2N_2ClNaS_2$ [M+Na$^+$]: 346.9686. Found: 346.9688.

Synthesis of P007H4[11]

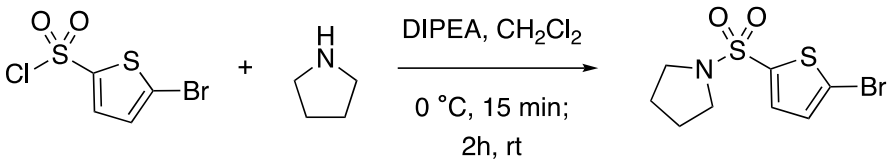

The sulfonyl chloride (1.05 g, 4 mmol) was dissolved in dichloromethane (1.0 mL) and the resulting solution was added dropwise to a round-bottom flask containing a stirred solution of pyrrolidine (657 µL, 8 mmol) and diisopropylethyllamine (1.5 mL, 8 mmol) in dichloromethane (10 mL) at 0 °C. The resulting reaction mixture was allowed to stir at 0 °C for 15 min and then allowed to warm to room temperature. After 2 h, the resulting solution was washed with 10 mL each of saturated sodium bicarbonate, water, 1 N HCl and brine. The organic layer was dried with magnesium sulfate, and solvent was removed under reduced pressure to give 1-((5-bromothiophen-2-yl)sulfonyl)pyrrolidine (**P007H4**). **^{1}H NMR (400 MHz, $CDCl_3$):** δ 7.30 (d, *J* = 4.0 Hz, 1H), 7.08 (d, *J* = 4.0 Hz, 1H), 3.29 – 3.22 (m, 4H), 1.85 – 1.74 (m, 4H). **^{13}C NMR (101 MHz, $CDCl_3$):** δ 137.98, 132.05, 130.47, 119.30, 48.20, 25.34. **HRMS (ESI):** Calculated for $C_9H_{10}BrNO_2S_2Na$ [M+Na$^+$]: 317.9229. Found: 317.9229.

Synthesis of P2065E16

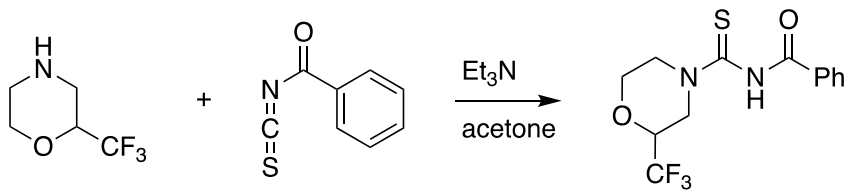

SI-1

To a flask purged and backfilled under nitrogen was added a solution of 2-trifluoromethyl-morpholine (100 mg, 0.522 mmol) in 0.5 mL dry acetone. Triethylamine (0.109 mL, 0.783 mmol) was added via syringe and the resulting solution allowed to stir at room temperature for 30 minutes. The solution was cooled to 0°C, and benzoyl isothiocyanate (0.702 mL, 0.522 mmol) was added dropwise. The resulting solution was allowed to stir for 30 min at 0°C and was then quenched with 1 mL water. The crude product was extracted with ethyl acetate (2 x 30 mL). The organic layers were combined, dried over anhydrous sodium sulfate, and concentrated under reduced pressure. The resulting crude product mixture was purified via SiO_2 column chromatography in 5:1 Hexanes:EtOAc to give N-(2-(trifluoromethyl)morpholine-4-carbonothioyl)benzamide (**SI-1**) in 62% yield[12]. **^{1}H NMR (400 MHz, $CDCl_3$):** δ 7.93 – 7.75 (m, 2H), 7.69 – 7.55 (m, 1H), 7.50 (t, *J* = 7.7 Hz, 2H), 5.10 (d, *J* = 94.4 Hz, 2H), 4.11 (s, 3H), 3.86 (s, 1H), 3.58 – 3.42 (m, 1H), 3.37 (dd, *J* = 13.4, 10.6 Hz, 1H).

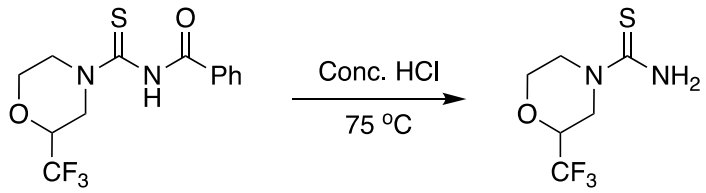

SI-1 **SI-2**

Concentrated HCl (2 mL) was added to **SI-1** (102.6 mg, 0.322 mmol). The resulting solution was allowed to stir for 1.5 hours at 75°C, then cooled to 0°C. Water (10 mL) was added, followed by 50% sodium hydroxide (5 mL). The aqueous phase was extracted with 1:1 ethyl acetate: petroleum ether (3 x 30mL). The organic layers were combined, washed with water (10 mL),

dried over anhydrous sodium sulfate, and concentrated under reduced pressure. The resulting crude product mixture was purified via SiO_2 column chromatography in 1:1 Hexanes:EtOAc to give 2-(trifluoromethyl)morpholine-4-carbothioamide (**SI-2**) in 51% yield[13]. **^{1}H NMR (400 MHz, $CDCl_3$):** δ 6.33 (s, 2H), 4.75 (d, *J* = 13.3 Hz, 1H), 4.30 (d, *J* = 13.4 Hz, 1H), 3.92 (dqd, *J* = 12.1, 6.0, 3.0 Hz, 1H), 3.64 (td, *J* = 11.6, 3.0 Hz, 1H), 3.25 (ddd, *J* = 13.5, 11.3, 3.6 Hz, 1H), 3.18 (dd, *J* = 13.4, 10.6 Hz, 1H).

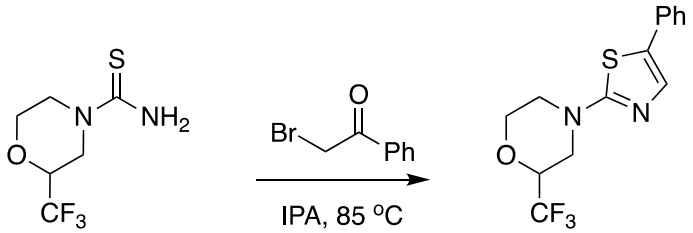

SI-2 **P2065E16**

SI-2 (35 mg, 0.164 mmol) and 2-bromoacetophenone (33 mg, 0.164 mmol) were dissolved in isopropanol (5 mL). The resulting solution was heated with stirring for four hours at 85°C. The reaction mixture was cooled to room temperature and concentrated under reduced pressure. The resulting crude reaction mixture was purified via SiO_2 column chromatography (hexanes/EtOAc) to give 4-(5-phenylthiazol-2-yl)-2-(trifluoromethyl)morpholine (**P2065E16**) in 24% yield[14]. **^{1}H NMR (400 MHz, $CDCl_3$):** δ 7.76 (d, *J* = 7.4 Hz, 2H), 7.32 (t, *J* = 7.7 Hz, 2H), 7.19 (d, *J* = 2.2 Hz, 1H), 6.79 (s, 1H), 4.10 – 3.91 (m, 3H), 3.75 (t, *J* = 15.1 Hz, 2H), 3.18 (dt, *J* = 38.2, 11.9 Hz, 2H). **HRMS (APCI):** Calculated for $C_{14}H_{13}F_3N_2OS$ [M^+]: 314.0701. Found: 314.0702.

Synthesis of P2065E16-CF_3

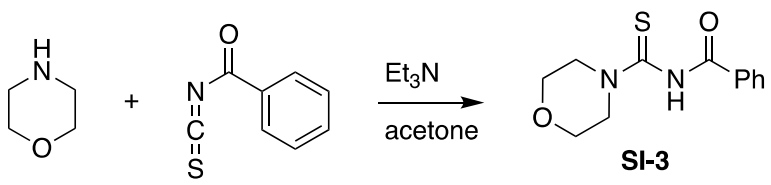

SI-3

Morpholine (1.0 g, 0.99 mL, 11.5 mmol) was added to dry acetone (10 mL) under nitrogen. Triethylamine (1.74 g, 2.40 mL, 17.2 mmol) was added via syringe and the resulting solution was allowed to stir at room temperature for 30 minutes. The resulting solution was cooled to 0°C, and benzoyl isothiocyanate (1.87 g, 1.54 mL, 11.5 mmol) was added dropwise. The resulting solution was allowed to stir for 30 min at 0°C and was then quenched with water (20 mL). The aqueous layer was extracted with ethyl acetate (2 x 30 mL). The organic layers were combined, dried over anhydrous sodium sulfate, and concentrated under reduced pressure. The resulting crude product mixture was purified via SiO_2 column chromatography in 3:1 Hexanes:EtOAc to give *N*-(morpholine-4-carbonothioyl)benzamide (**SI-3**) in 57% yield. **^{1}H NMR (400 MHz, $CDCl_3$):** δ 8.55-8.50 (m, 1H), 7.81 (d, J = 7.6 Hz, 2H), 7.57 (t, J = 7.6 Hz, 1H), 7.46 (t, J = 7.6 Hz, 2H), 4.20 (s, 2H), 3.85 – 3.77 (m, 4H), 3.63 (s, 2H).

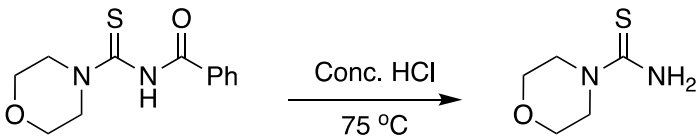

SI-3 **SI-4**

Concentrated HCl (4 mL) was added to **SI-3** (169 mg, 0.675 mmol). The resulting solution was heated with stirring for 1.5 hours at 75°C, then cooled to 0°C. Water (15 mL) was added, followed by 50% sodium hydroxide (10 mL). The aqueous phase was extracted with 1:1 ethyl acetate: petroleum ether (3 x 30 mL). The combined organic layers were dried over anhydrous sodium sulfate and concentrated under reduced pressure to provide morpholine-4-carbothioamide (**SI-4**) in 33% yield (no purification was necessary). **^{1}H NMR (400 MHz, $CDCl_3$):** δ 7.42 (s, 2H), 3.67 (t, *J* = 4.8 Hz, 4H), 3.52 (t, *J* = 4.8 Hz, 4H).

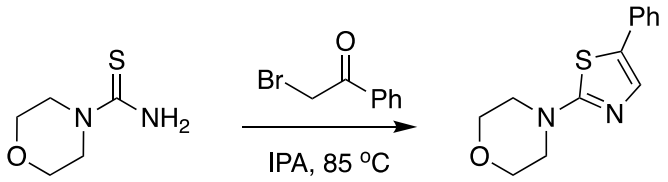

SI-4 **P2065E16-CF$_3$**

SI-4 (123 mg, 0.84 mmol) and 2-bromoacetophenone (167 mg, 0.84 mmol) were dissolved in isopropanol (5 mL). The resulting solution was heated with stirring for four hours at 85°C. The reaction was cooled to room temperature and concentrated under reduced pressure to give 4-(5-phenylthiazol-2-yl)morpholine (**P2065E16-CF$_3$**) in quantitative yield. δ 7.82 – 7.76 (m, 2H), 7.37 (t, *J* = 7.6 Hz, 2H), 7.31-7.25 (m, 2H), 3.70 (t, *J* = 4.9 Hz, 4H), 3.46 (t, *J* = 4.8 Hz, 4H). **^{13}C NMR (101 MHz, DMSO-*d*$_6$)**: δ 170.99, 148.82, 133.74, 129.02, 128.49, 126.42, 103.43, 65.71, 48.87. **HRMS (EI):** Calculated for $C_{13}H_{14}N_2OS$ [M$^+$]: 246.0827. Found: 246.0839.

References

1. van Kessel, J.C., Ulrich, L.E., Zhulin, I.B. & Bassler, B.L. Analysis of activator and repressor functions reveals the requirements for transcriptional control by LuxR, the master regulator of quorum sensing in Vibrio harveyi. *mBio* **4**(2013).
2. Hustmyer, C.M. et al. Promoter Boundaries for the luxCDABE and betIBA-proXWV Operons in Vibrio harveyi Defined by the Method Rapid Arbitrary PCR Insertion Libraries (RAIL). *J Bacteriol* **200**(2018).
3. Newman, J.D. & van Kessel, J.C. Purification of the Vibrio Quorum-Sensing Transcription Factors LuxR, HapR, and SmcR. *Methods Mol Biol* (2020).
4. Newman, J.D., Russell, M.M., Gonzalez-Gutierrez, G. & van Kessel, J.C. The DNA binding domain of the *Vibrio vulnificus* SmcR transcription factor is flexible and recognizes diverse DNA sequences. *bioRxiv* (2020).
5. Trott, O. & Olson, A.J. AutoDock Vina: improving the speed and accuracy of docking with a new scoring function, efficient optimization, and multithreading. *J Comput Chem* **31**, 455-61 (2010).
6. De Silva, R.S. et al. Crystal structure of the Vibrio cholerae quorum-sensing regulatory protein HapR. *J Bacteriol* **189**, 5683-91 (2007).
7. Kim, Y. et al. Crystal structure of SmcR, a quorum-sensing master regulator of Vibrio vulnificus, provides insight into its regulation of transcription. *J Biol Chem* **285**, 14020-30 (2010).
8. Morris, G.M. et al. AutoDock4 and AutoDockTools4: Automated docking with selective receptor flexibility. *J Comput Chem* **30**, 2785-91 (2009).

9. Kim, B.S. et al. QStatin, a Selective Inhibitor of Quorum Sensing in Vibrio Species. *MBio* **9**(2018).
10. Nishida, H.A., Yasuyoshi; Hirase, Keizo. Preparation of thiophene and pyrazole derivatives and related analogous as acid secretion inhibitors and antiulcer agents. (ed. LIMITED, T.P.C.) (2009).
11. Keil, S.U., Matthias; Wendler, Wolfgang; Glien, Maike; Matter, Hans; Munson, Harry Randall, Jr. Preparation of sulfonamides with heterocycle and oxadiazolone headgroups with PPARδ or PPARδ and PPARα agonist activity. (ed. SANOFI-AVENTIS) (2010).
12. Buckley, D.I.D., Gregory; Wagman, Allan S.; Evanchik, Marc; McDowell, Robert S. Heterocyclic modulators of lipid synthesis. (ed. 3-V BIOSCIENCES, I.) (2018).
13. Shreykar, M. & Sekar, N. Resonance induced proton transfer leading to NIR emission in coumarin thiazole hybrid dyes: synthesis and DFT insights. *Tetrahedron Letters* **57**, 4174-4177 (2016).
14. Li, H. et al. Discovery of small-molecule inhibitors selectively targeting the DNA-binding domain of the human androgen receptor. *J Med Chem* **57**, 6458-67 (2014).

Figure 1

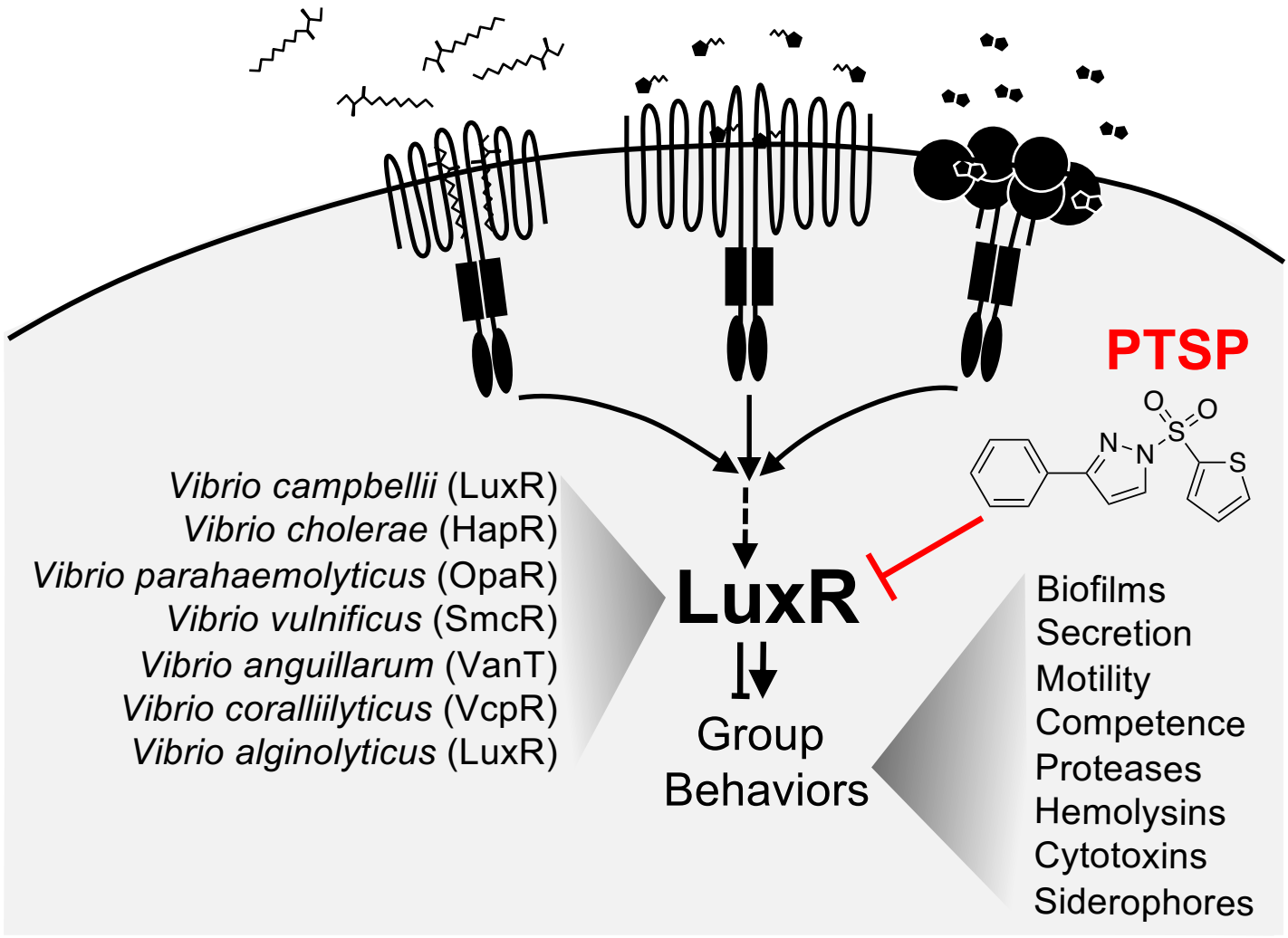

Figure 2

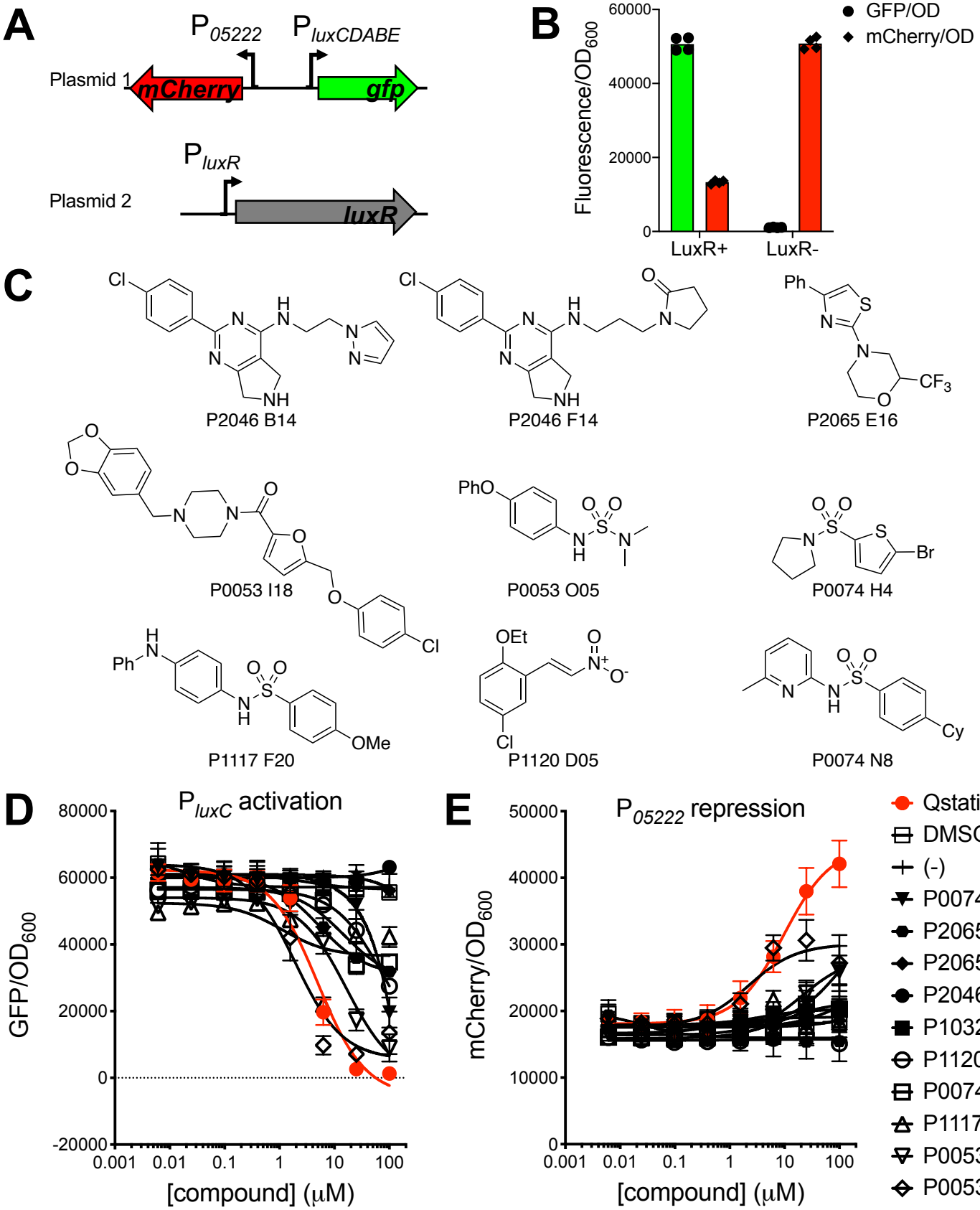

Figure 3

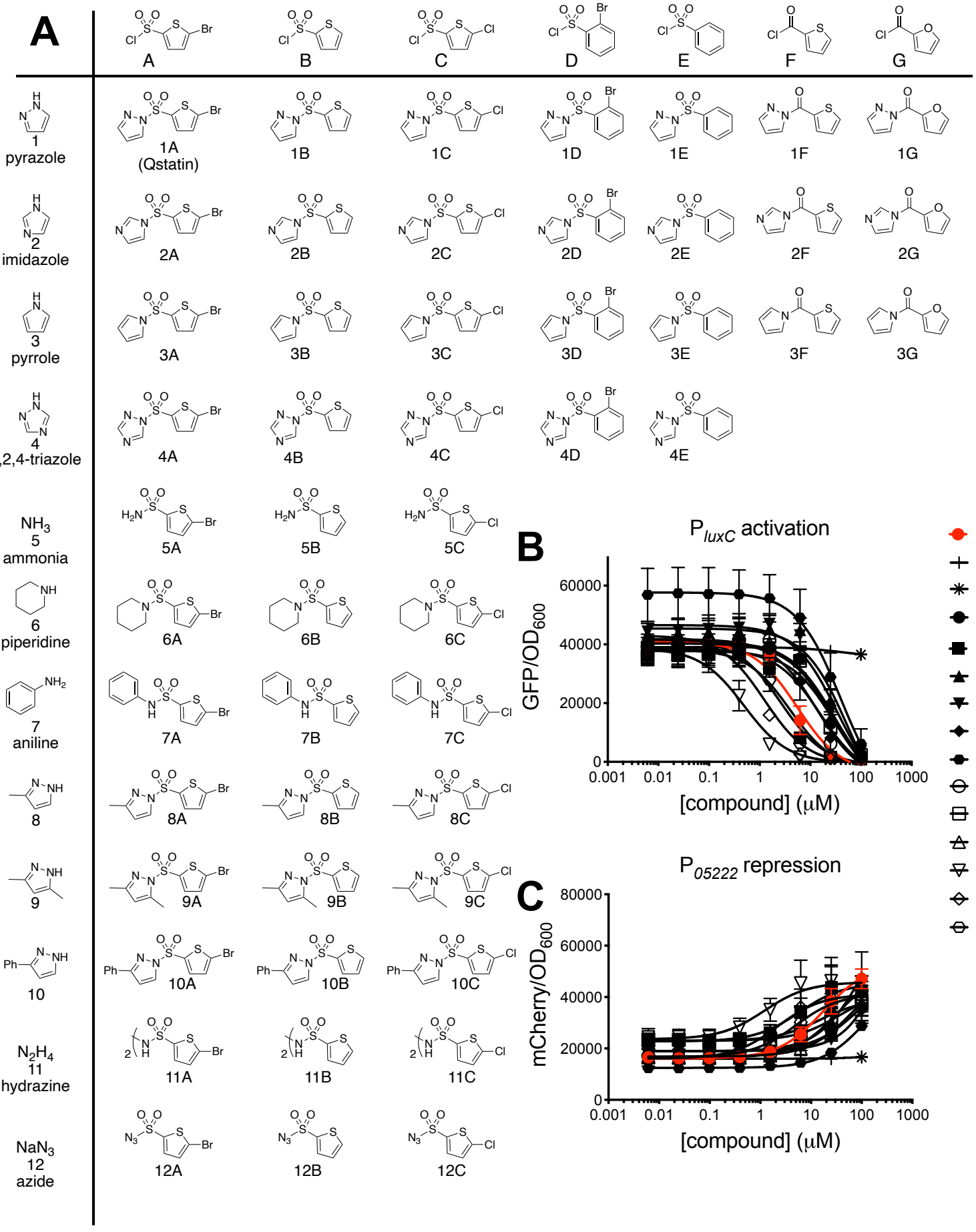

Figure 4

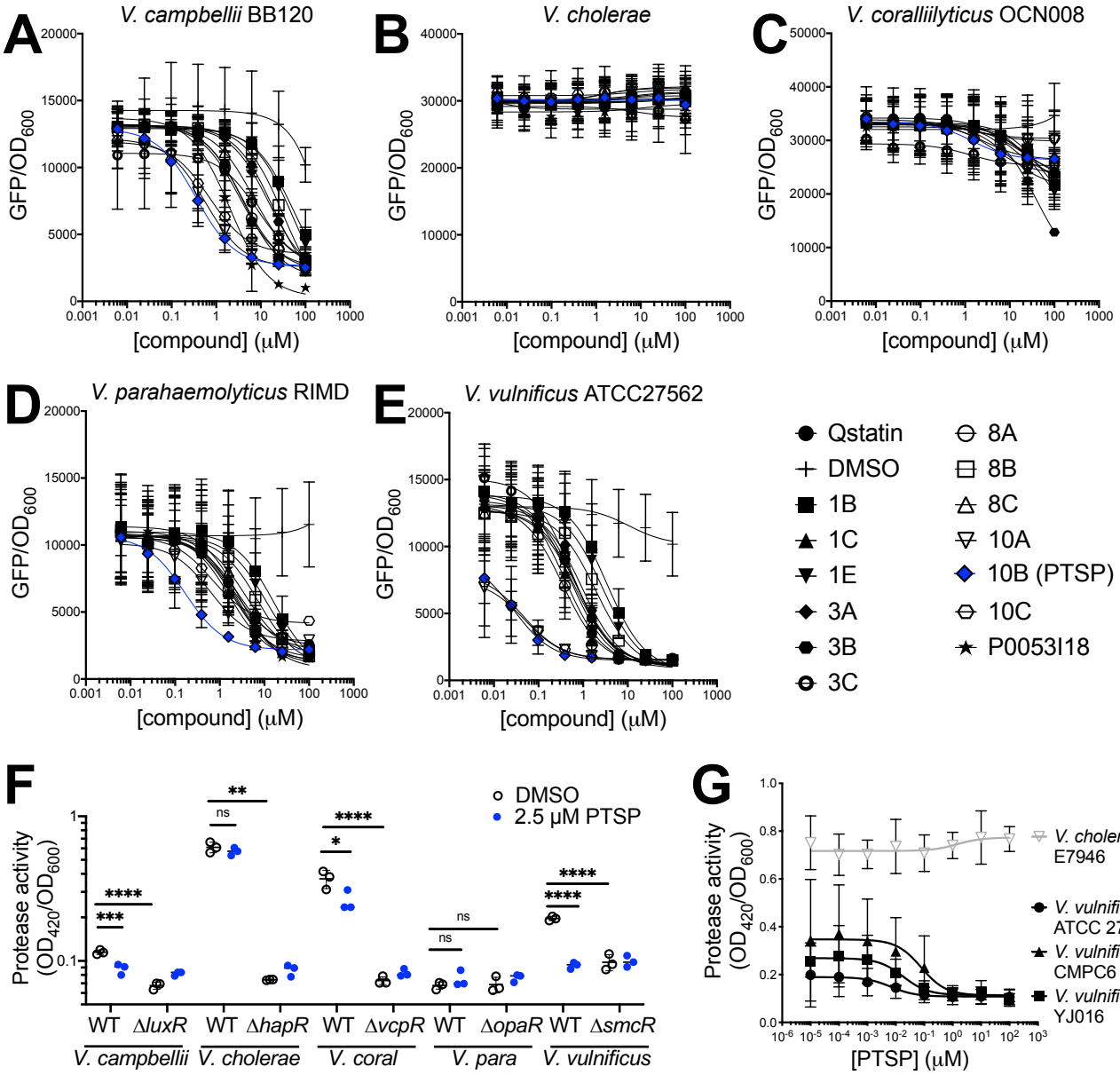

Figure 5

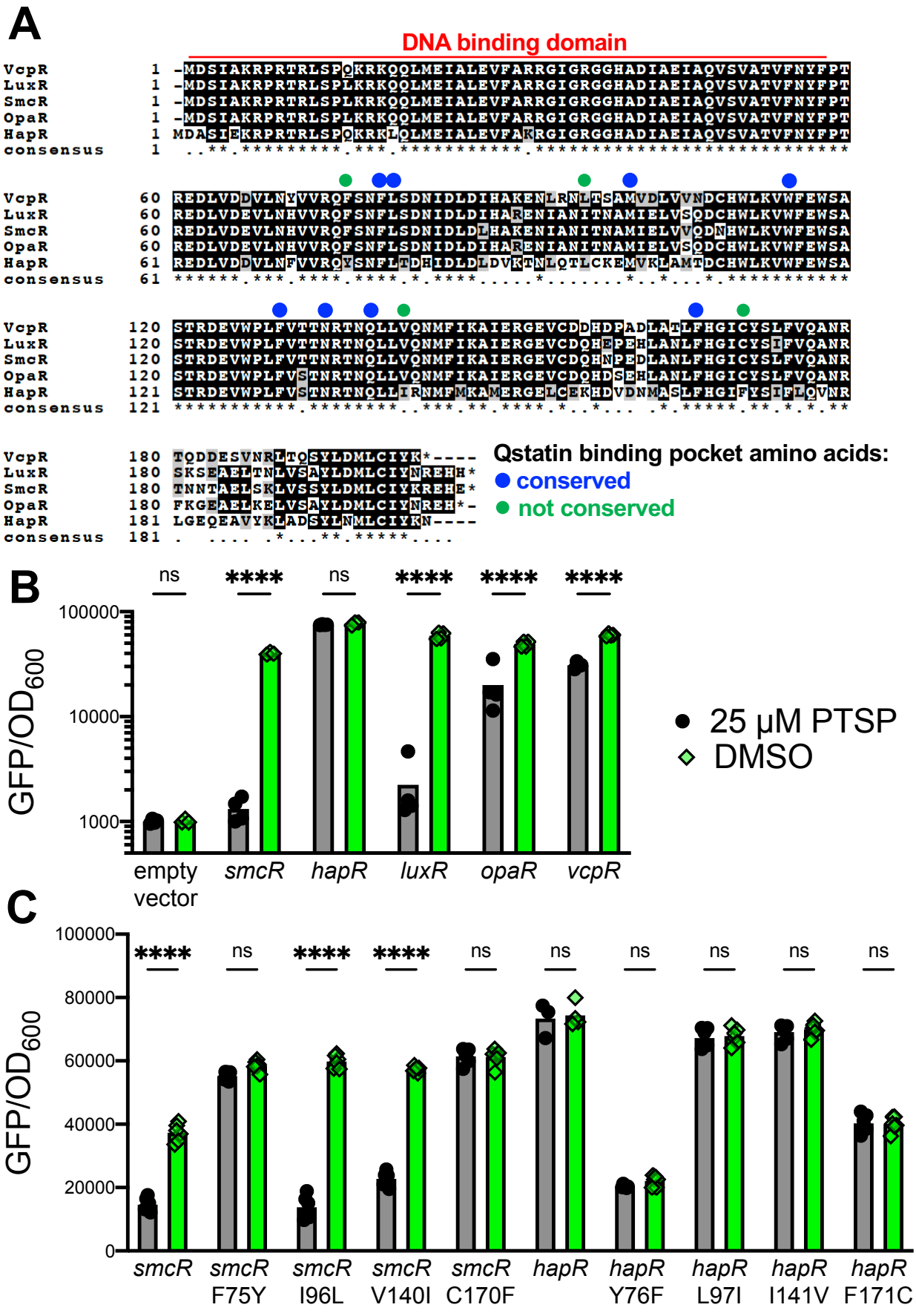

Figure 6